Fuel 341 (2023) 127726

Contents lists available at ScienceDirect

Fuel

journal homepage: www.elsevier.com/locate/fuel

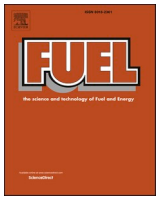

Full Length Article

Bimetallic cobalt catalysts promoted by La_2O_3 for the production of high-calorie synthetic gas

Andreina Alarcón [a,b], Olatz Palma [a], Elena Martín Morales [a], Martí Biset-Peiró [a], Teresa Andreu [b], Jordi Guilera [a,b,*]

[a] Catalonia Institute for Energy Research (IREC), Jardins de les Dones de Negre 1, 08930 Sant Adrià de Besòs, Spain
[b] Facultat de Química. Universitat de Barcelona, Martí i Franquès, 1, Barcelona 08028, Spain

ARTICLE INFO

Keywords:
Synthetic fuel synthesis
C_1-C_4 hydrocarbons
CO_x hydrogenation
bimetallic Co-X catalyst
La_2O_3 promoter
Heating value

ABSTRACT

A new catalytic route for the production of a high-calorie synthetic gas (40–60 MJ/Nm^3), composed by C_1-C_4 hydrocarbons, has industrial interest for gas applications and locations with high heating requirements. In this work, a series of bimetallic Co-X (X = Ni, Pt and Fe) catalysts supported on La_2O_3 promoted Al_2O_3 micro-spheres were evaluated using both CO_2 and CO carbon sources under mild temperature (T = 200–300 °C), moderate pressure (P = 10 bar·g) and relatively high gas hourly space velocity (40,000 N mL/g_{cat}·h). Experimental results proved that the incorporation of nickel as a second metal is beneficial for high-calorie gas application. Besides, catalytic results showed that the utilization of CO as carbon source is beneficial in both conversion and C_1-C_4 hydrocarbon selectivities. Co-Ni presented the most interesting results, leading to a heating value of 57.9 MJ/Nm^3 (40.01 % CH_4 and 50.04 % C_2-C_4 hydrocarbon) at 250 °C through CO hydrogenation. The enhanced catalytic performance achieved over bimetallic Co-Ni was attributed to CoNi alloy catalytic activity, high reducibility (73.82 %), active metal content (9.65x10^{-4} mmol/g) and appropriate acid-basic sites for CO_x activation. In contrast, the conversion of CO_2 to high-calorie gas was found to be more challenging and lower gas heating values were achieved (39.73 MJ/Nm^3). In this case, an adapted reactor concept using a dual bimetallic catalyst and different reaction conditions is hereby proposed to shift selectivity towards the targeted products. This findings represent a step forwards in catalytic engineering for the development of high-calorie synthetic gas reactors.

1. Introduction

The combination of green hydrogen with biogenic carbon dioxide feedstocks generates synthetic fuel with low carbon footprint [1]. So far, two main synthetic fuel routes have been extensively proposed: Power-to-Gas (Sabatier), which produces almost pure CH_4; and Power-to-Liquid (Fischer-Tropsch), which aims to mimic the composition of current fossil liquid hydrocarbons (C_5^+), as gasoline, kerosene, light and heavy diesel. In contrast, there is not a well-established low-carbon fuel route to produce light alkanes (C_2-C_4), which are now present in the fossil-based natural gas (1–10 %) and in liquefied petroleum gas (LPG) [2]. Indeed, C_2-C_4 hydrocarbons are vastly used (>300 MMT annually [3]) as fuel in heating appliances, cooking equipment and vehicle transport. Therefore, a novel catalytic route favouring C—C coupling for the generation of a high-calorie synthetic gas (HC-SG) is of special interest for several applications and different locations.

A mixture of CH_4 and C_2-C_4 hydrocarbons composes the so-called HC-SG, which exhibits a higher heating value (~57.72 MJ/Nm^3) [4] than fossil natural gas (42–46 MJ/Nm^3) and much higher than from the product of Sabatier synthesis (37.74 MJ/Nm^3) [5]. As emerging fuel, there are no well-defined standards of HC-SG properties. As reference, a mixture exceeding 40 MJ/Nm^3 can be considered a high-calorie gas, as it can be comparable with current natural gas specifications. To satisfy this standard, HC-SG should contain at least 5–15 vol% of C_2–C_4 paraffin hydrocarbons [6].

In principle, HC-SG could be produced alternatively from CO and CO_2 feedstocks. In this sense, the main reactions involved in the HC-SG synthesis depend on the carbon source. The direct pathway for the production of hydrocarbons is through the so-called modified Fischer-Tropsch reaction (m-FT, Eq. (1)). Nevertheless, an indirect pathway occurs when the CO_2 molecule is converted to CO by means of the reverse Water Gas Shift reaction (rWGS, Eq. (2)), which generates the

* Corresponding author.
E-mail address: jguilera@irec.cat (J. Guilera).

https://doi.org/10.1016/j.fuel.2023.127726
Received 28 July 2022; Received in revised form 20 January 2023; Accepted 5 February 2023
Available online 13 February 2023

intermediate for the production C_1-C_4 hydrocarbons, similar to the Fischer-Tropsch reaction (FT, Eq. (3)). The relative extension of the abovementioned reactions (Eqs. (1) - (3)) depends on (i) the nature of the catalytic material and (ii) the reaction conditions, which need to be controlled to achieve the desired selectivity [7].

$$nCO_2 + 3nH_2 \leftrightharpoons C_nH_{2n} + 2n\ H_2O \qquad \Delta H^{\circ}_{298K} = -128\,\frac{KJ}{mol} \tag{1}$$

$$CO_2 + H_2 \leftrightharpoons CO + H_2O \qquad \Delta^{\circ}_{298K} = +41\,\frac{KJ}{mol} \tag{2}$$

$$nCO + (2n+1)H_2 \leftrightharpoons C_nH_{2n+2} + n\ H_2O \qquad \Delta H^{\circ}_{298K} = -166\,\frac{KJ}{mol} \tag{3}$$

Cobalt (Co) [8] and iron (Fe) [910] are suitable catalysts for the production of HC-SG. Cobalt-based catalysts have the best compromise between performance and cost for the synthesis of hydrocarbons from H_2/CO mixtures [1112]. Qi et al. indicated that the synthesis of highly dispersed Co catalysts requires the initial formation of very small CoO or Co_3O_4 crystallites [13]. The formation of these small oxide clusters, in turn, requires strong interactions between the support and the Co precursor. Besides, Lee et al. reported that Co-based catalyst performance towards the production of C_2-C_4 hydrocarbons can be enhanced by the incorporation of a second metal. Recently, the effect of Mn and Ru on Co-based catalysts was evaluated [14]. They found that Mn is able to modify the surface acidity, and promote carbon-rich environment on the surface, which resulted in an increase of the C_2-C_4 yield. Concerning Ru, they claimed that this metal phase is able to increase the reducibility of catalysts, resulting in a high activity at a lower temperature. In other works, the combination of Co and Fe was also reported. Co-Fe/Al_2O_3 catalysts were more selective to light hydrocarbons (C_2–C_4), with respect to monometallic Co-based catalysts [15]. Furthermore, it was observed that the formation of FeCo alloy can destabilize the iron carbide phase and suppress the carbon chain growth [16].

In addition to Co-Fe, other bimetallic catalysts have been proposed for the production of HC-SG from syngas, such as Fe-Ni [2], Fe-Zn [4], Fe-Cu [17] and Fe-Pd [18]. In the case of bimetallic Fe-Zn catalyst, Zn exhibited hydrogen spillover ability, which increases CO hydrogenation. Most recently, catalytic systems based on CeO_2−Pt@mSiO_2−Co[19], $Ni_{3x}Co_xO_4$ [20], as well as tri-metallic Co-Fe-Ni catalysts [21] have been studied for the production of HC-SG. In this latter, Kim et al. concluded that the metal dispersion and reducibility were enhanced in the presence of nickel, leading to an improved catalytic activity.

Those studies reported that the incorporation of a second metal increases the fraction of reduced metal and, consequently, its activity to HC-SG. Despite efforts to elucidate the effect of the second metal on the HC-SG reaction, some major key issues related to hydrocarbon C_2-C_4 promotion remained elusive. The adsorption trend of CO_x over cobalt catalyst should play a significant role in the product distribution in HC-SG and diffuse reflectance infrared Fourier transform spectroscopy (DRIFTS) studies can give valuable information about adsorption trends and formation of intermediates during the thermocatalytic reaction. In this direction, the beneficial role of lanthanide metal oxides on Al_2O_3 supports for CO_2 methanation and Fischer-Tropsch reaction using nickel [22] and cobalt [23] catalysts was recently reported. In this aspect, lanthanide promotion on bimetallic cobalt catalyst would be able to incorporate moderate basic sites, and thus, facilitate CO_x adsorption, which arises as an interesting strategy to increase the production of HC-SG.

The main goal of this work is to propose a La_2O_3 promoted bimetallic catalytic system able to increase HC-SG production from CO and CO_2 carbon sources under moderate pressure. As well, to identify the most favourable reaction temperature conditions for each catalyst and carbon source. To the best of our knowledge, this catalytic system has not reported for HC-SG synthesis in the open literature. With this aim, we developed a series of catalysts based on Co-X/La_2O_3-Al_2O_3, using Ni, Pt and Fe as promising second active metal phases (X). The promoted support, monometallic and bimetallic catalysts were evaluated at 200–300 °C, 10 bar·g and relatively high gas flowrates. In-situ DRIFTS experiments were used to elucidate the role of the second metal when exposed to the different carbon sources. The heating values of the obtained gas mixtures and potential reaction engineering design for HC-SG production is hereby discussed.

2. Experimental

2.1. Catalyst synthesis

A series of micro-catalysts with particle sizes between 200 and 300 μm, were prepared by a melting infiltration method previously proposed by our group [24]. Catalyst samples were composed by 80 wt% of the promoted support (65 wt% of γ-Al_2O_3 and 15 wt% of La_2O_3) and 20 wt% of metal active phase (10 wt% Co + 10 wt% second metal Ni, Pt or Fe for bimetallic and Co for monometallic). The bimetallic catalysts were denoted as Co-Ni, Co-Pt and Co-Fe. The content of the promoter phase (15 wt%) was selected according to a previous work [22].

For the impregnation of a 5 g-batch, the salt precursors (cobalt + second metal + promoter) were added to the alumina support, mixed and dissolved on a rotary evaporator at 120 °C for 1 h. In the case of Co-Pt catalyst, 3.9 mL of water were added to guarantee the dissolution of the $PtCl_4$ metal precursor. Then, the temperature was reduced to 90 °C and vacuum was applied until complete evaporation, 4 h approximately. The impregnated material was kept at 110 °C in an atmospheric oven overnight. Subsequently, the catalysts were calcined at 450 °C for 30 min, with a heating ramp of 1 °C/min.

Chemicals used for catalyst synthesis were γ-Al_2O_3 in shape of microspheres with particle diameters d_p = 200–300 μm (Puralox) as support, salt precursor of lanthanum (III) nitrate hexahydrate [$La(NO_3)_3{\cdot}6H_2O$] (99.99 % purity, Aldrich) as promoter, and salt precursors of cobalt (II) nitrate hexahydrate [$Co(NO_3)_2{\cdot}6H_2O$] (100 % purity, Emsure), nickel (II) nitrate hexahydrate [$Ni(NO_3)_2{\cdot}6H_2O$] (98 % purity, Alfa Aesar), tetra platinum (IV) chloride [$PtCl_4$] (99.99 % purity, Alfa Aesar), iron (III) nitrate nonahydrate [$Fe(NO_3)_3{\cdot}9H_2O$] (98 % purity, Sigma-Aldrich) as active phases.

2.2. Catalyst characterization

The microstructure morphology and elemental composition analysis of the catalysts were studied using scanning electron microscopy (Zeiss Auriga 60) equipped with an energy dispersive X-rays spectroscopy detector (EDX, Oxford Instruments), respectively. SEM images were recorded using the SE2 detector at a power beam range of 3 kV, working distance (WD) of 5.2 mm and a magnification of 100 X. In the case of SEM-EDX analysis, these were conducted at 20 kV using a copper standard for the system calibration. The chemical composition analysis was restricted to Co, Ni, Pt, Fe, Al, La and O, and it was calculated as the average over five measurements (standard deviation σ ± 1) on different regions for each sample.

N_2-physisorption (adsorption/desorption) measurements were determined at liquid nitrogen temperature using an automated TriStar II 3020-Micromeritics analyzer. Samples were degassed at 90 °C for 1 h, and then at 250 °C for 4 h in a FlowPrep 060-Micromeritics. Brunauer-Emmett-Teller (BET) method was used to calculate the BET surface area for a relative pressure (P/P_o) range of 0.05–0.30. Barrett-Joyner-Halenda (BJH) method was applied to desorption branch of the isotherms to determine the average pore size and the total pore volume, which was calculated from the maximum adsorption value at P/P_o = 0.999.

The true densities of catalysts were studied using a helium pycnometer (Ultrapyc pycnometer 1200e, Quantachrome Instruments). Experiments were carried out on a large sample cell that was filled only the 75 % of its volume to ensure accuracy (±0.02). Prior to

measurements, the cell loaded with catalyst was transferred to the sample chamber. True density values were estimated by the average of collected data points from three runs measured at 20 psi.

Micrometrics Autochem II equipment was used to study the reducibility of the catalysts in the programmed temperature range from 25 to 800 °C. For the analysis, 0.1 g of each sample was placed in a U-shaped quartz reactor and supported on quartz wool. A mixture of 10 vol% H_2/Argon (50 NmL/min) was used as a reducing gas in the tests, while the temperature was raised from 25 °C to 800 °C with a ramp of 10 °C/min. The signal of H_2 consumption was detected by a thermal conductivity detector (TCD). The amount of reduced metal oxides to metal species was calculated by integrating the reduction peaks in the H_2-TPR profiles and expressed as a percentage of consumption to reduce the metal species in the catalysts.

XRD patterns were collected within the 2Θ range 20-80° in a Bruker type XRD D8 Advance A25 diffractometer using a Cu Kα radiation (λ = 1.5406 Å), a voltage of 40 kV, a current of 40 mA and a step size of 0.05° (with 3 s duration at each step). Dataset was normalized to guarantee a proper interpretation of the results. For calcined sample, the average crystallite size of Co_3O_4 was estimated using the Scherrer's equation at 2Θ = 36.9°. D=(Kλ/βCosΘ), where λ is the X-ray wavelength, β is the full width of the diffraction line at half maximum (FWHM), and Θ is the Bragg angle. On the other hand, the average crystallite sizes of the metallic Co (Co^0) and alloys (CoX^0) were estimated at 2Θ = 44.21° for Co [1 1 1], 44.50° for CoNi [1 1 1], 41.55° for CoPt [1 1 1], and 44.83° for CoFe [1 1 0].

The metal dispersion (D) was calculated from the average metal crystallite size (M = Co^0 and CoX^0), by using Eq. (4). It is important to mentioned that the applicability of this equation is viable only if we assumed that the promoter phase and/or second metal phase is not present in the catalytic composition. In other words, all the catalysts should be considered monometallic Co-based catalysts with spherical uniform metal crystallite with a site density of 14.6 atoms/nm^2.

$$D(\%) = 96/d(M^0) \tag{4}$$

2.3. Catalytic tests

The reactions for study of catalytic activity were conducted on a laboratory fixed-bed rector with a diameter of 13 mm and a length of 305 mm (Microactivity Reference, PID Eng&Tech). The tubular stainless-steel reactor was placed inside a ceramic chamber, which was heated by an electrical resistance. The reaction temperature was monitored using a K-type thermocouple placed in the middle of the catalytic bed. Experiments were carried out using 300 mg of catalyst, which was diluted with 3 g of silicon carbide of similar particle size (355 μm) to guarantee an isothermal catalytic bed. The mixture reactants (H_2 (99.999 %, Linde), CO_2 (99.999 %, Linde) and CO (99.999 %, Linde)) were supplied by mass flow controllers (MFC, Bronkshorst) at 200 N mL/min. H_2:CO_2 = 3 and H_2:CO = 3 molar ratio was set. Thus, experiments were carried at 40.000 N mL/g_{cat}·h of gas hourly space velocity. Pressure was set at the reactor outlet by an automatic valve at 10 bar·g.

After reaction, the products passed through a cold liquid–gas separator (5 °C), where water was trapped, and then the dry flow was measured by a mass flow meter (MF, Bronkshorst). The composition of the dry gas was analysed by a micro-chromatograph Aglient Technologies 490 Micro GC Biogas Analyzer model. It was equipped with three channels, the first channel (CP-Sil 5 CB) analysed C_3H_6, C_3H_8, C_4H_{10} and C_{5+}; the second channel (CP-PoralPLOT U) analysed CO_2, C_2H_4 and C_2H_6; and the third channel (CP-Molsieve 5A) analysed H_2, CH_4 and CO.

Prior to reaction, catalysts were in-situ reduced under H_2 flow (100 N mL/min) at 500 °C for 3 h using a heating ramp of 1 °C/min, and then cooled to 50 °C with the same ramp rate. The catalytic activity was evaluated in a range of temperature from 200 to 300 °C, with an interval of 50 °C.

The conversion of CO_x and C_1-balance selectivity toward the hydrocarbon products were calculated using Eqs. (5) - (7):

$$\text{Conversion of } CO_x\ (\%) = \left(1 - \frac{CO_{x,out}}{CO_{x,in}}\right)\cdot 100 \tag{5}$$

where Co_X (x = 1 for CO and 2 for CO_2) represents the molar flow rate of the species in the inlet and outlet gas.

$$\text{Selectivity } C_nH_m(\%) = \left(\frac{n\cdot C_nH_m}{\sum (n\cdot C_nH_m)_{out} + CO_{x,out}}\right)\cdot 100 \tag{6}$$

where C_nH_m is the hydrocarbon of carbon n and hydrogen m (m = 2n + 2 for paraffins y m = 2n for olefins).

$$\text{Selectivity to } CO_x(\%) = \left(\frac{CO_{x,out}}{\sum (n\cdot C_nH_m)_{out} + CO_{x,out}}\right)\cdot 100 \tag{7}$$

At the outlet, products such as CO, CO_2 and H_2 species were not considered as part of the HC-SG. Therefore, the heating values (Eq. (8)) for HC-SG were only calculated based on the NIST Chemistry WebBook data for heat of combustion of the methane and C_2-C_4 hydrocarbons (CH_4:891 MJ/mol; C_2H_4:1411 MJ/mol; C_2H_6:1561 MJ/mol; C_3H_6:2058 MJ/mol; C_3H_8: 2220 MJ/mol; C_4H_{10}: 2878 MJ/mol) [5].

$$\text{Heating Value}\left(\frac{MJ}{Nm^3}\right) = \sum_{n=1}^{4}\left(\frac{\text{Volume fraction}\cdot \text{Heat of combustion}\left(\frac{MJ}{mol}\right)}{\text{Specific volume}\left(\frac{Nm^3}{mol}\right)}\right) \text{ of the hydrocarbon of carbon number n} \tag{8}$$

2.4. In-situ DRIFTS

DRIFTS measurements were performed on a Bruker-Vertex70 spectrophotometer equipped with a MCT detector and a high temperature reaction cell (Harrick Praying Mantis) with two ZnSe windows. Prior to the experiments, the samples were reduced at 500 °C in the reaction cell under an Ar/H_2 flux. A flux of 20 mL/min with an Ar:H_2:CO_2 ratio of 12:3:1 was applied for the reaction with CO_2 and a flux of 40 mL/min was applied for the reaction with CO with an Ar:H_2:CO ratio of 12:3:1. The reactions were studied in the temperature range of 50–300 °C, at intervals of 50 °C. Background spectra were recorded under Ar at each temperature.

3. Results and discussion

3.1. Physicochemical properties of the series of catalysts

A series of catalysts based on Co-X/La_2O_3-Al_2O_3 were prepared, characterized and evaluated. The physicochemical properties of the γ-Al_2O_3 support, the promoted La_2O_3 support, the monometallic Co catalyst and the bimetallic Co-Ni, Co-Pt and Co-Fe catalysts are described as follows.

SEM-EDX analysis of Co-X/La_2O_3-Al_2O_3 revealed the presence and distribution of the metals related to the active phases (Co-X; X = Ni, Pt, Fe) and promoter phase (La), thus confirming metal impregnation. As a representative example, SEM-EDX mapping of bimetallic Co-Ni catalyst is shown in Fig. 1. As it can be observed, Ni, Co and La elements were distributed uniformly over the support. Furthermore, the SEM image of the Ni-Co indicated that the topological characteristics (size and shape) of the bimetallic catalyst were analogous to those of the γ-Al_2O_3 support, i.e. micro-spherical catalysts with particle diameters between 200 and 300 μm. An approximatio of the elemental composition of the series of catalysts is presented in Table 1. The percentage in weight of the bimetallic active phase (Co-X = 17–21 wt%) and the metal oxide promoter (La_2O_3 = 12–16 wt%) phase were fairly close to the nominal ones. Therefore, EDX data suggest a good and consistent impregnation of whole series of catalysts.

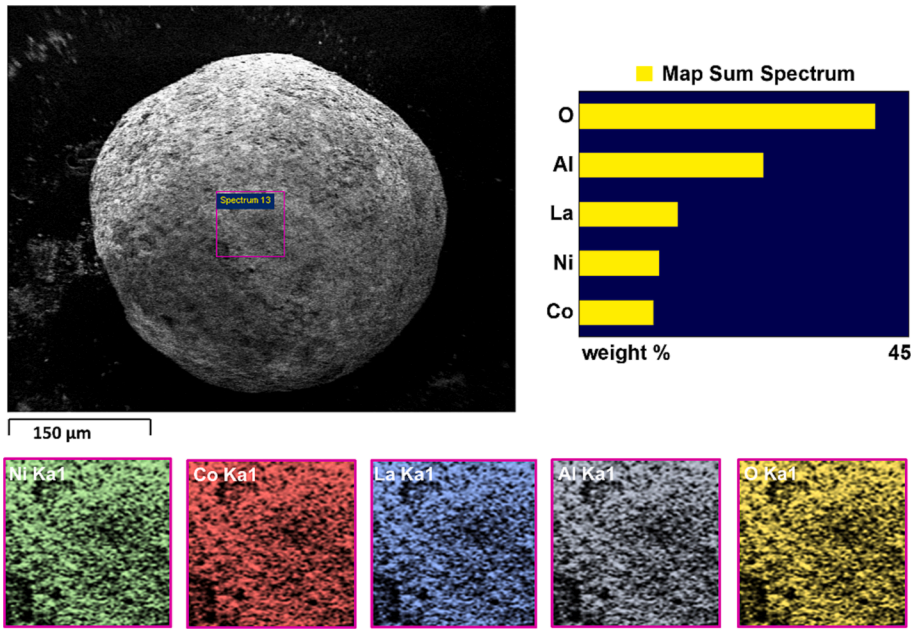

Fig. 1. SEM-EDX mapping of the bimetallic Co-Ni catalyst.

Table 1
Elemental composition and textural properties of the catalysts.

Sample	SEM-EDX							N_2-physisorption			
	Elemental composition [wt. %]							True Density	BET surface area	Pore volume	Pore diameter
	Co	**X**	**La**	**Al**	**O**	**Co-X**	**La_2O_3**	**[g/mL]**	**[m^2/g]**	**[cm^3/g]**	**[nm]**
Support	–	–	–			–	–	3.33	194	0.45	10.70
Promoted support	–	–				–	15.32	3.37	189	0.39	6.54
Co	16.72	–	10.99	27.47	44.86	16.72	12.89	3.70	107	0.23	6.71
Co-Ni	10.15	10.90	13.49	25.08	40.38	21.05	15.82	3.90	114	0.24	6.71
Co-Pt	9.73	8.68	12.60	26.19	42.79	18.41	14.78	3.78	129	0.23	6.68
Co-Fe	8.47	8.52	10.46	27.40	44.98	16.99	12.48	3.68	127	0.25	7.07

The nitrogen adsorption/desorption isotherms of the catalysts were type IV classification (see Figure SI1) [25]. As expected, the γ-Al_2O_3 support presented larger BET surface area, pore volume and pore diameter than the promoted support and the rest of catalysts. The addition of La_2O_3 promoter together with the active phases Co or Co-Ni, Co-Pt and Co-Fe in γ-Al_2O_3 support resulted in a generalized reduction in their textural properties of the catalysts caused by the incorporation of non-porous metal-oxides on a porous support. Fig. 2 suggests that between Co and Co-X samples a narrow distribution in the mesoporous range was achieved, peaking higher than 6.71 nm. The true density of the catalysts was always increased after metal loading to the support.

The H_2-TPR profiles are displayed in Fig. 3. At the studied reduction temperature range (T = 25–800 °C), the promoted support composed by

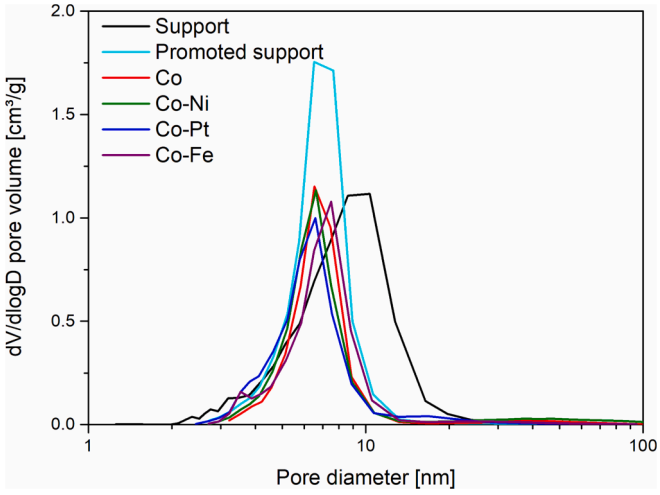

Fig. 2. Pore diameter of the catalysts.

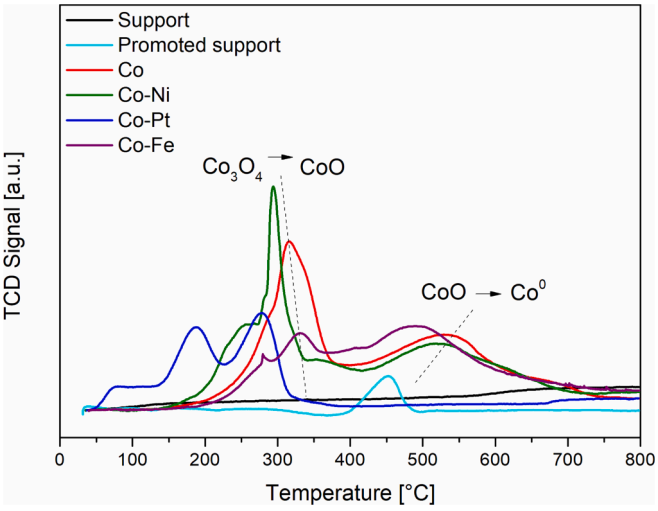

Fig. 3. TPR profiles of the catalysts.

Table 2
Structural properties of the catalysts.

Sample	XRD			H_2-TPR		
	[a]Co_3O_4 [nm]	[b]Co^0 [nm]	[b]CoX [nm]	Degree of reduction at 500 °C [%]	Metal dispersion [%]	Active metal content [10^{-6} mol/g]
Support	–	–	–	–	–	–
Promoted support	–	–	–	18.34	–	–
Co	15.87	9.05	–	68.6	10.61	10.32
Co-Ni	13.05	–	14.12	73.82	6.79	9.65
Co-Pt	15.12	–	16.42	100	5.85	7.65
Co-Fe	10.74	–	10.43	67.71	9.20	7.75

[a] Co_3O_4 crystallite sizes were estimated from calcined catalysts.
[b] Co^0 and CoX crystallite sizes were estimated from reduced catalysts.

La_2O_3-γ-Al_2O_3 showed one characteristic peak at around 450 °C, which was related to the reduction of the La_2O_3 promoter, whereas the reduction of γ-Al_2O_3 support was not identified at this temperature range. The main broad peaks for monometallic Co catalyst were categorized in two zones: a low temperature zone (250–375 °C) related to the reduction of Co_3O_4 to CoO and a high temperature zone (420–600 °C) related to the final reduction of CoO to Co^0 [26].

Bimetallic catalysts exhibited a different reduction behaviour than monometallic Co. H_2-TPR profiles of bimetallic catalysts presented a deviation to lower temperatures and new reduction peaks appeared. As for Co-Ni, a shoulder located around 200–275 °C was detected and assigned to the reduction of NiO to Ni^0 [27]. Compared to other bimetallic catalysts, the reduction of the PtO_x species over Co-Pt catalyst was identified at much lower temperature, <200 °C [28]. Regarding to Fe-Co catalyst, the reduction peaks located around 280 °C and 400 °C were assigned to the reduction of Fe_xO_y species [29]. According to these results, it can be inferred that cobalt oxide particles have a different interaction degree with the promoted La_2O_3-Al_2O_3 support and strong Co-X bonds benefit Co reduction. It was well reported that La_2O_3 on Co/Al_2O_3 increased catalyst reducibility [30]. On the other hand, the total percentage of catalyst reduction is presented in Table 2. At the selected reduction temperature of 500 °C, all bimetallic catalysts, except Co-Fe, showed a high reducibility (≥74 %) compared to the monometallic Co analogue (≈69 %). Furthermore, as the total reduction was only achieved for Co-Pt, it was inferred that the reduced catalyst structure of Co, Co-Ni and Co-Pt were composed by a mixture of metallic oxide particles (CoO, La_2O_3-Al_2O_3) and active metal sites in a single form (Co) for the monometallic Co and alloy form (CoNi, CoFe, CoPt) for bimetallic catalysts.

The X-ray diffraction patterns of the series of catalysts in their calcined states, are reported in Figure SI2. The addition of La_2O_3 did not give rise to crystalline phases and only contributed to the reduction in the intensity of the γ-Al_2O_3 reflections. The [220], [311], [222], [400], [511] and [440] crystal planes corresponding to γ-Al_2O_3 phase (JCPDS:00–010-0425) were identified at 2θ = 32.35, 37.90, 39.11, 46.15, 61.25 and 67.25°, respectively. In addition to γ-Al_2O_3, Co_3O_4 phase was detected in all the Co-based catalysts. The reflections of the Co_3O_4 phase (JCPDS:00–043-1003) were recognized at 2θ = 31.24, 36.96, 44.83, 59.17 and 65.18°, corresponding to the [220], [311], [400], [400] and [440] crystal planes. In the bimetallic catalysts, the Co_3O_4 phase was shifted to the left (see Figure SI3), indicating a change in the lattice parameter of this phase. The lattice CO_3O_4 deviation can be caused by its interaction with the NiO_x, PtO_x, and Fe_xO_y atoms of the second metal phase. Furthermore, no well-defined reflections linked to the oxide phase of the second metal were detected in the bimetallic catalysts. The absence of these reflections indicates that the metal oxide species could be present in an amorphous phase, in a highly dispersed crystalline phase or in the formation of a mixed oxide. Therefore, in order to confirm the reduction of metal oxides and the formation of CoX alloys, the structural properties of all catalysts in their reduced state were also evaluated.

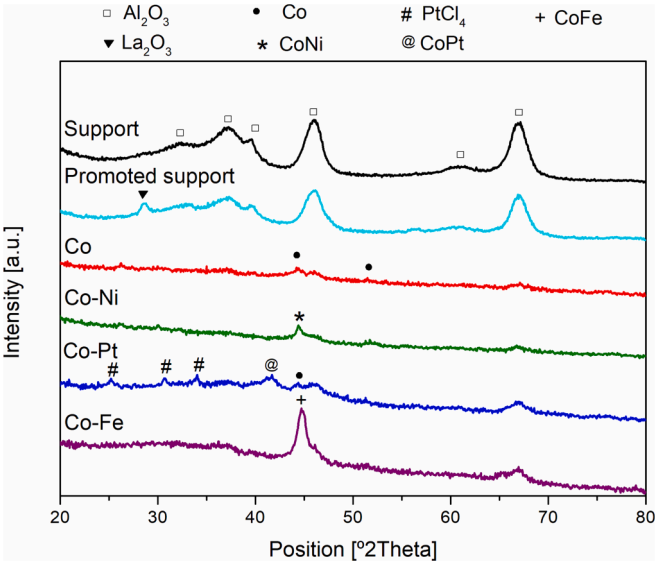

Fig. 4. XRD pattern of the series of reduced catalysts.

XRD patterns of the reduced catalysts are shown in Fig. 4. After the reduction of the samples, Al_2O_3 and La_2O_3 phases related to the support and promoter were respectively detected. The new reflection of La_2O_3 phase (JCPDS:00–050-0602) was located at 2θ = 28.59°. Besides Al_2O_3 and La_2O_3 phases, it was expected the presence of CoO, as most of the catalysts were not totally reduced at 500 °C, according to TPR results. However, this metal oxide phase cannot be identified over the reduced samples. The absence of this reflection was attributed to its highly dispersed crystalline phase. In contrast, metallic Co was identified in both mono and bimetallic catalysts. The [111] and [200] crystal planes of the Co phase (JCPDS:00–015-0806) were detected at 2θ = 44.21 and 51.52°, respectively. Interestingly, in the reduced bimetallic catalysts, new reflections attributed to the formation of CoX alloys were identified. The main characteristic reflections appearing at 44.50°, 41.66° and 44.83° correspond to CoNi [111] (JCPDS:00–010-8308), CoPt [101] (JCPDS:00–043-1358) and CoFe [110] (JCPDS:00–044-1483), respectively. In particular, in the reduced Co-Pt, three reflections were additionally located at 25.81, 30.59 and 34.06° and assigned to $PtCl_4$ [131], [240] and [241] crystal planes (JCPDS:00–030-0886); indicating that the chemical precursor was still present in Co-Pt catalyst.

The metallic crystallite sizes of Co and alloys (CoNi, CoPt and CoFe) were calculated from XRD patterns using the Scherrer's equation. A crystallite size of 9.05 nm was estimated for the reduced Co catalyst. For the reduced bimetallic catalysts, the interaction of Co and the second metal (X: Ni, Pt and Fe) over promoted La_2O_3-Al_2O_3 support led to the formation of CoX crystallites with sizes higher than 10 nm, suggesting that the structure of the bimetallic Co-X phases were preferentially conformed by CoX alloys. As it is shown in Table 2, CoPt crystallite size (16.42 nm) was much higher than that estimated for CoNi (14.12 nm) and CoFe (10.43 nm), causing an inferior metal dispersion over the bimetallic catalysts. In particular, the low Pt dispersion identified over Co-Pt can be also influenced by the presence of $PtCl_4$. This compose has measurable vapor pressure and is mobile, and therefore susceptible to segregation [31]. On the other hand, the active metal content (>$8{\cdot}10^{-6}$ mol/g) estimated from SEM-EDX, XRD, and TPR data, suggested that the percentage of reduction of the catalysts is a key point for their performances.

3.2. Catalytic performance to HC-SG

The catalytic performance of the different catalyst formulations, the support and the promoted support was evaluated on the synthesis of HC-SG from both CO_2 and CO as carbon sources at different reaction temperatures.

3.2.1. CO_2 as carbon source

All the catalysts, Co, Co-Ni, Co-Pt and Co-Fe, were active at the selected conditions and CO_2 conversions always increased with temperature (see Fig. 5). Overall, the catalytic activity followed this order: Co-Ni > Co > Co-Fe > Co-Pt ≫ promoted support. Co-Ni was the most active, achieving a maximum CO_2 conversion of 49.31 %. Therefore, the strategy of adding a second active phase only seems to be beneficial in the case of Ni, in the view of the CO_2 conversion results.

The main product species measured were CO, CH_4, and C_2-C_4, whereas large C_{5+} hydrocarbons were not detected from CO_2 hydrogenation[323232]. In contrast, the La_2O_3 promoted support was not able to form hydrocarbons. Fig. 6 shows the product distribution of the different catalysts and temperature conditions, and it reveals that low temperatures were preferred to produce C_2-C_4 hydrocarbons. It can be observed that the monometallic Co catalyst was the less selective towards C_2-C_4 hydrocarbons. Therefore, this catalytic behaviour revealed that the incorporation of the second metal was a positive strategy in terms of selectivity to C_2-C_4 hydrocarbons. At the other end, a very different mixture, which was composed by CO and C_2-C_4 hydrocarbons species were formed over Co-Pt catalyst. In the case of Co-Ni, the most active catalyst, it was preferentially selective to form CH_4. A similar behaviour was identified for bimetallic Co-Fe, which displayed a drop in C_2-C_4 hydrocarbon selectivity as temperature increased.

Fig. 7 shows the DRIFTS spectra recorded over the Co-based catalysts at a temperature of 250 °C using CO_2 as carbon source. At this temperature, methane is the main product of the hydrogenation reaction, confirmed by its characteristic peaks at 3015 and 1314 cm^{-1} present in all the spectra, which is well aligned with the results obtained in the catalytic experiments. There are, however, different species adsorbed at the surface of the catalysts at every temperature that account for the different reactivity observed in the catalytic experiments. Over monometallic Co (see Figure SI4), besides generation of methane above 200 °C, carbonate species (1700–1340 cm^{-1}) and accumulation of physisorbed water (3240 cm^{-1}) were also observed on the surface of the catalysts. At 250 °C, a new peak was identified at 1340 cm^{-1} and assigned to monodentate carbonate species. This characteristic peak was also observed, although less intense, over bimetallic catalysts. It should be noted that in Co-Ni, release of methane is observed from 150 °C (see Figure SI5), proving the high activity of this catalyst towards the methanation of CO_2. At the same time, the ill-defined bands between 1700 and 1400 cm^{-1} are attributed to the presence of carbonate and carboxylates species adsorbed on the support [33]. A comparable behaviour is observed for the Fe-Co catalyst, which displays similar and less intense peaks (see Figure SI6). On the other hand, when using the Co-Pt catalyst, coordination of CO on Pt sites is indicated by the presence of a peak at 2070 and a shoulder at 1990 cm^{-1} [34] (see Figure SI7). This observation is in line with the catalytic experiments, as the Co-Pt catalyst is the only one that significantly yielded CO as product at all the temperatures studied. It can be therefore inferred that the Co-Pt bimetallic catalyst facilitates the rWGS reaction [35], which explains the lower production of methane of this catalyst. Two broad bands centred at 1560 and 1375 cm^{-1}, that decrease in intensity at higher temperatures, are attributed to the adsorption of formate species on the promoted support [36].

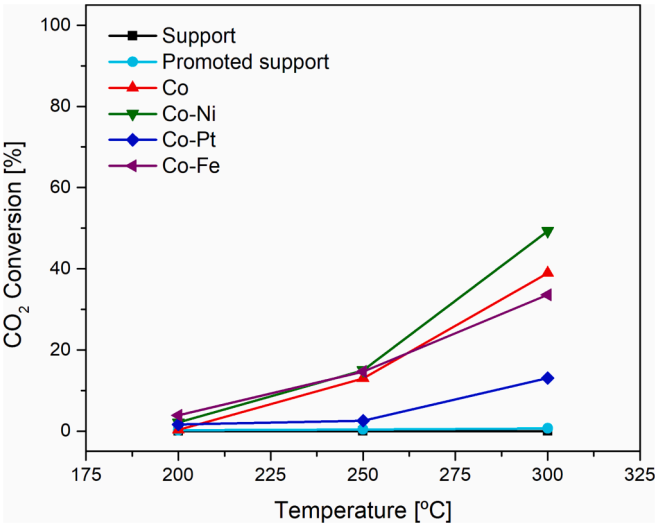

Fig. 5. CO_2 conversion as a function of the temperature.

3.2.2. CO as carbon source

Catalytic performance using CO as carbon source is displayed in Fig. 8. In comparison to CO_2, the use of CO as a carbon source was very advantageous in terms of gas reactivity. The achieved CO conversion was very dependent on the temperature and ranged between 0.89 and 90.65 %, much higher values with respect to CO_2 conversion (<50 %). In the present reaction system, monometallic Co was more active than the bimetallic Co-X catalysts, implying that Ni, Pt and Fe are less active when CO is used as carbon source. These results are in correlation with the literature since cobalt-based catalysts are usually found as an active catalyst for mixtures H_2/CO in the FTS process [37]. CO conversion on the studied catalysts at all the used temperatures complies with the following order: Co > Co-Ni > Co-Fe > Co-Pt ≫ promoted support.

Selectivity from CO hydrogenation is presented in Fig. 9. Besides conversion, selectivity to C_2-C_4 hydrocarbons was also enhanced by the utilization of CO as a carbon source. Species such as CO_2, CH_4, C_2-C_4 and even C_5 were detected in the evaluated temperature range of 200–300 °C. In this case, the promoted support was preferentially selective to form small amounts of CO_2. The best results of selectivity to C_2-C_4 hydrocarbons were achieved over bimetallic catalysts at 250 °C, being the Co-Ni the most promising compared to Co-Pt and even more than Co-Fe. However, its important to note that in terms of hydrocarbon selectivity, the Co-Fe shows competitive values at the higher tested temperature of 300 °C, implying that Fe was beneficial to form C_{2+} hydrocarbons and Ni was also favourable to form CH_4. Therefore, the addition of a second metal as a catalyst design strategy was proved to improve the selectivity towards the formation of C_2-C_4 hydrocarbons. Similar to CO_2 hydrogenation, low temperatures are preferred to favour C_2-C_4 hydrocarbon production.

Fig. 10 shows the DRIFTS spectra collected for the Co-based catalysts at a reaction temperature of 250 °C. In the hydrogenation of CO, peaks related to hydroxyl groups (400–3500 cm^{-1}) and CO species adsorbed on Lewis acid sites (1606 and 1573 cm^{-1}) and Brønsted acid sites (1651 cm^{-1}) of the La_2O_3-Al_2O_3 [3839] support were identified. Furthermore, release of hydrocarbons is observed by the characteristic ν(CH) modes of methyl (CH_3) and methylene (CH_2) groups at 2958, 2924 and 2850 cm^{-1} [40 41], respectively, as well as methane at 3015 and 1305 cm^{-1} (see Figure SI8). Compared to monometallic Co, new peaks attributed to CO species adsorbed on Lewis acid sites (1629, 1620, 1610, 1492 and 1450) and strong Brønsted acid sites (1639 cm^{-1}) were identified over Co-Ni [3839]. The production of CH_4 and hydrocarbons (2990 and 2968 cm^{-1} (methyl), 2896, 2873 and 2862 cm^{-1} (methylene)) was mainly visible at temperatures above 200 °C [42] (see Figure SI9). Formate species detected 1585 cm^{-1} were related to the formation of methane as it exhibited an analogous behaviour to the methane band. In addition, the signal at 2360 cm^{-1} detected at all the temperatures studied is attributed to formation of gaseous CO_2, which indicates that the water gas shift (WGS) reaction takes place from very low temperatures. At

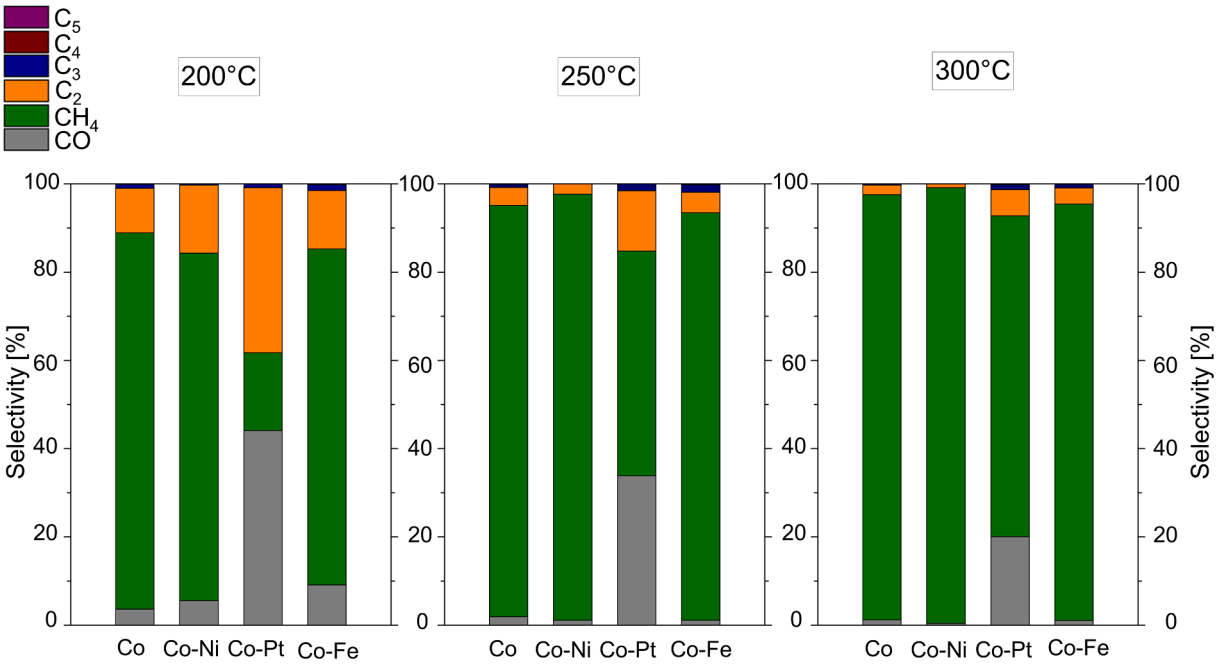

Fig. 6. Selectivity from CO_2 of Co-based catalysts as a function of the temperature.

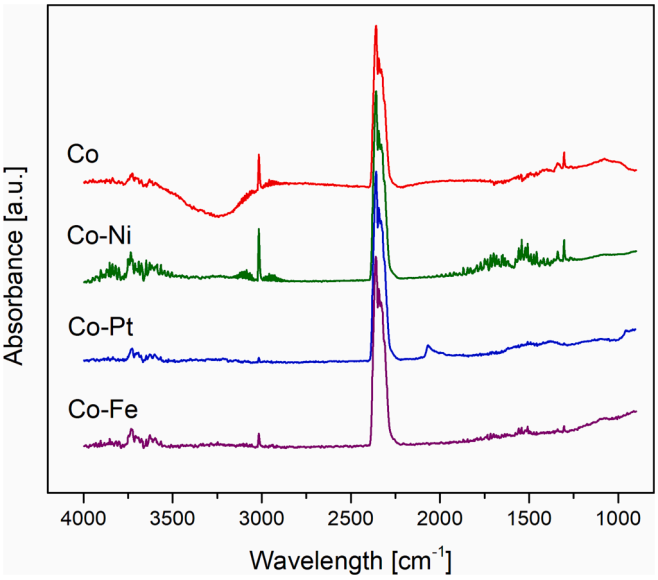

Fig. 7. DRIFTS spectra of the Co-based catalysts at 250 °C under an Ar:H_2:CO_2 feed.

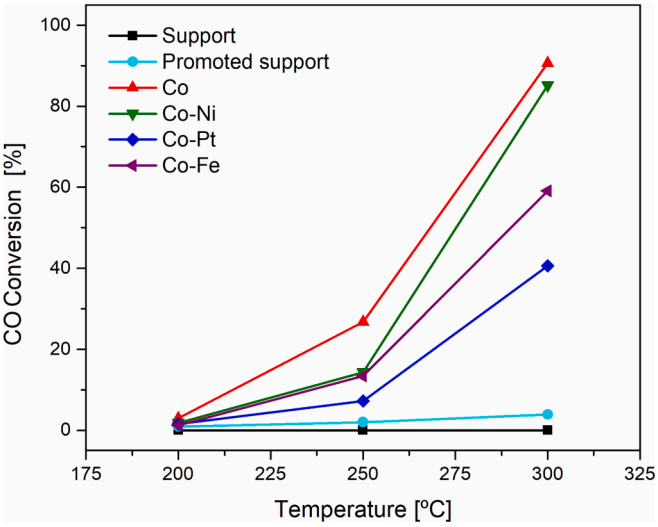

Fig. 8. CO conversion as a function of the temperature.

300 °C, the signal of CO_2 significantly increases in intensity while that of methane was maintained, and those of methyl and methylene groups even slightly decrease, which could suggest a strong competition between the WGS reaction and the FT reaction at this temperature. When the Co-Fe catalyst is used, formation of CO_2 and water is observed by the broad band centred at 3250 cm^{-1}. The series of multiple peaks between 1700 and 1200 cm^{-1} can be assigned to carbonate species adsorbed on the surface of the promoted support (see Figure SI10). For the Co-Pt catalyst, adsorption of linear CO species on Pt sites of different natures is detected by the presence of a peak at 2080 cm^{-1} and a shoulder at 2057 cm^{-1} [43], appearing at higher temperatures (see Figure SI11). Generation of methane and longer hydrocarbons is observed at temperatures above 200 °C by the appearance of peaks at 3015, 2960, 2930 and 2870 cm^{-1}, along with a broad band centred at 3240 cm^{-1} and attributed to water, which is product of the C_2-C_4 formation reactions. Again, gaseous CO_2 is observed by the peaks at 2354 and 2320 cm^{-1}, as a result of the water gas shift reaction.

According to these results, the promising production of CH_4 and C_2-C_4 hydrocarbons over bimetallic Co-X can be attributed to CO adsorbed on Lewis and Brønsted active sites. For the promoted support (See Figure SI12), the peaks associated with the CO adsorption on La_2O_3-AL_2O_3 surface around 1700–1400 cm^{-1} was enhanced as temperature increased from 200 to 300 °C. However, with the addition of the second metal phase, the peaks of Lewis and Brønsted were different, indicating that the acid strengths differed between monometallic and bimetallic samples. Between Co and Co-Ni, the presence of new peaks and the difference in intensities indicates a difference in the amount of acid sites between, and thus in the formation of C_2-C_4 hydrocarbons (see Figure SI13).

In summary, the main highlights of the catalytic results obtained at the selected conditions are the following:

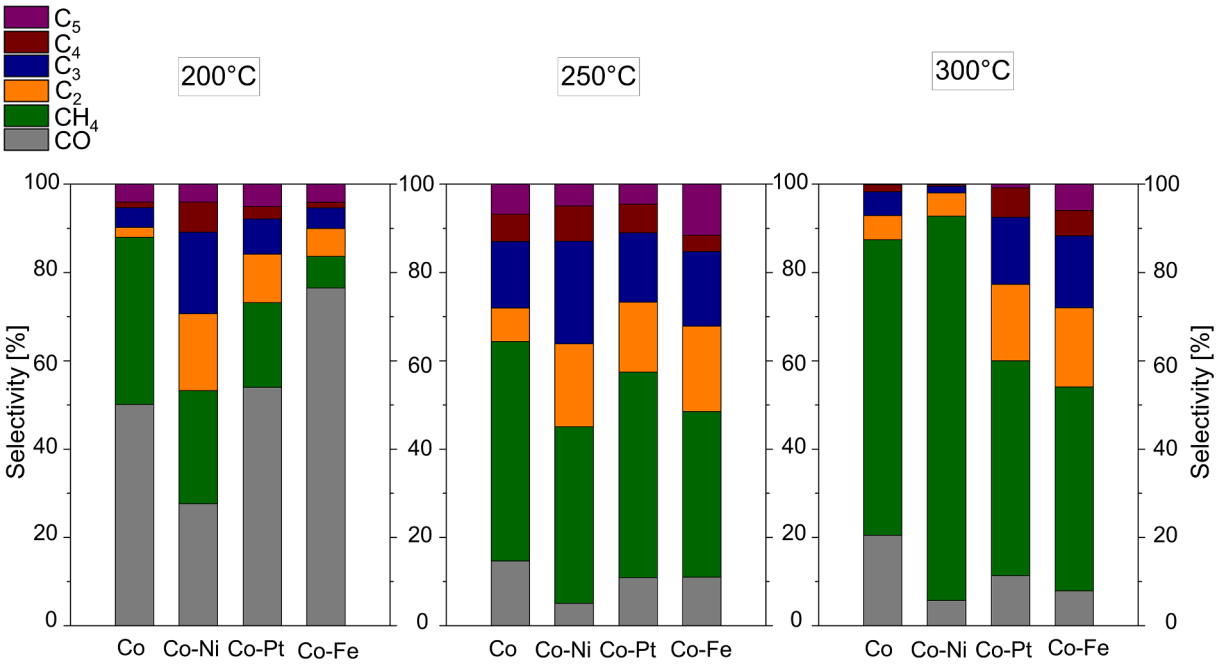

Fig. 9. Selectivity from CO of Co-based catalysts as a function of the temperature.

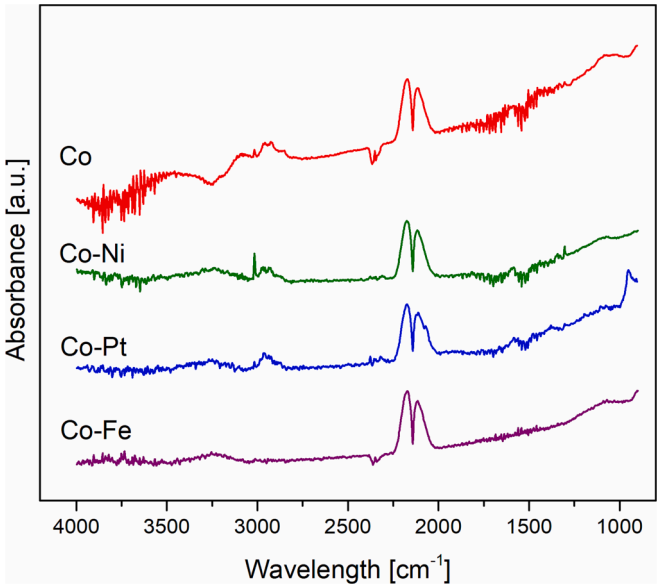

Fig. 10. DRIFTS spectra of the Co-based catalysts at 250 °C using an Ar:H_2:CO feed.

i) In both cases (CO_2 or CO), competitive C_2-C_4 hydrocarbons selectivities were achieved using as low as possible temperatures at the expense of the conversion.
ii) CO as carbon source was beneficial in terms of activity and C_2-C_4 hydrocarbons selectivity.
iii) Co-Ni was identified as the most promising catalyst as led to an enhanced production of CH_4 and C_2-C_4 hydrocarbon species, compared to the rest of Co-X bimetallic and monometallic Co catalyst.
iv) DRIFTS experiments revealed that the chemical properties of promoted support have close relationships with the CO_x activation as different carbon species adsorbed on Lewis and Brønsted active sites can be identified over the La_2O_3 promoted Co-X based catalysts. Furthermore, it was confirmed by DRIFTS that the addition of the second metal promoted the formation of species CH_4 and C_2-C_4 hydrocarbons. The most promising HC-SG production detected over bimetallic Ni-Co can be attributed to the long-chain hydrocarbons typically formed on Co and effectively hydrocracked by Ni, which is known to be active in C — C bond cleavage [44].

Therefore, the characterization of the materials indicated that the addition of Ni and Pt on Co-based catalyst improved its reducibility, while the addition of Fe was noticed to enhance its metal dispersion. Furthermore, the modification of the Al_2O_3 support with La_2O_3 promotes the formation of CoX alloys, favouring the hydrogenation reaction at low temperatures and controlling methane and hydrocarbon selectivity production. Finally, it can be claimed that the high catalytic activity and preferential selectivity to C_4 and C_2-C_4 hydrocarbons of the Co-Ni was due to the formation of CoX alloy, high reducibility (73.82 %) and suitable active metal content ($9.65x10^{-6}$mmol/g).

3.3. Product distribution and heating values

A summary of the product distribution over the series of catalyst at the most promising reaction temperature is presented in Table 3. Product distribution at the rest of temperatures can be found in supporting information, Table SI1. Competitive HC-SG mixtures were successfully achieved during the hydrogenation of CO. In particular, a gas product with a HHV of 57.90 MJ/Nm^3 was achieved under CO hydrogenation and using the bimetallic Ni-Co as catalytic material at 250 °C. The HHV of the generated HC-SG was in the range of the reported ones (<57.72 MJ/Nm^3), which operated at very low gas hourly space velocities (GHSV = 6,000 NmL/g_{cat}·h) and using non-promoted bimetallic Fe-Zn/Al_2O_3 [4] and tri-metallic Ni-Co-Fe/Al_2O_3 systems [21]. Therefore, the addition of La_2O_3 to the traditional bimetallic system based on Co-X/Al_2O_3 was found to be positive, since higher GHSVs can be used during the hydrogenation of CO [23].

In contrast, the use of CO_2 as carbon source seems more challenging. In this case, the maximum HHV was also achieved over bimetallic Ni-Co (39.73 MJ/Nm^3) at the lowest temperature, 200 °C, being significantly lower than the use of CO as carbon source. These results also reveal the lower CO_2 conversion values compared to CO as carbon source. As

Table 3
Product distributions over the series of catalysts using CO_2 and CO as carbon sources.

Sample	CO_2 as carbon source							CO as carbon source						
	T = 200 °C							T = 250 °C						
	CO_2 conversion [%]	CO	CH_4 selectivity [%]	C_2-C_4	C_5	Y_{HC-SG} Yield [%]	HHV [MJ/Nm^3]	CO conversion [%]	CO_2	CH_4 selectivity [%]	C_2-C_4	C_5	Y_{HC-SG} Yield [%]	HHV [MJ/Nm^3]
Support	–	–	–	–	–	–	–	–	–	–	–	–	–	–
Promoted support	0.12	100.00	0.00	0.00	0.00	–	0.00	2.01	97.66	0.00	2.34	0.00	0.05	1.49
Co	0.33	3.65	85.28	11.07	0.00	0.32	39.46	26.71	14.63	49.74	28.80	6.81	20.98	44.75
Co-Ni	2.14	5.53	78.76	15.69	0.00	2.02	39.73	14.31	5.05	40.01	50.04	4.89	12.89	57.90
Co-Pt	1.63	44.07	17.66	38.27	0.00	0.91	31.22	7.19	10.86	46.57	38.04	4.52	6.08	49.78
Co-Fe	3.84	9.11	76.12	14.76	0.00	3.49	38.52	13.40	11.01	37.49	39.94	11.57	10.38	46.31

Reaction conditions: GHSV = 40,000 NmL/g_{cat}·h, H_2:CO_2 or CO molar ratio of 3, and P = 10 bar·g.

previously described, Co-Pt catalyst favors CO and C_2-C_4 formation. However, experiments on CO indicated that part of the generated CO would be converted back to CO_2, therefore reducing the global CO_2 conversion. According to these results, it seems that the utilization of a single catalyst seems not feasible for CO_2 hydrogenation as the selectivity to C_2-C_4 is limited or rWGS reaction to CO is favoured, restricting the HHV obtained.

The implementation of a dual catalytic bed configured by two different Co-X catalysts can be an interesting strategy when using CO_2 as carbon source, as reported by Gao et al. [45]. In the present HC-SG reactor engineering concept, the catalytic bed would be composed by two zones, which will work to different reaction conditions. A schematic representation is shown in Figure SI14. The first one is denoted as the CO_2 decomposition zone and designed to favour the conversion of CO_2 to CO and CH_x (x = 1,2,3) species. In this zone, the bimetallic catalyst based on Co-Pt can be used to guarantee the reactive mixture composition. As the temperature is a key reaction condition to achieve high CO selectivities, the temperature of the catalytic bed in this zone can be fixed at 200 °C. After the first zone, in the same catalytic bed, a second zone denoted as the HC-SG formation zone is designed to favour the conversion of CO to HC-SG (CH_4 and C_2-C_4 hydrocarbons). As Ni-Co exhibited the most promising HC-SG production, this can be the bimetallic catalyst implemented in the second zone. Compared to the previous one, the hydrogenation of CO to CH_4 and C_2-C_4 hydrocarbons over Co-Ni should be performed at a higher temperature 250 °C.

Unfortunately, the inefficient catalytic performance under the H_2/CO_2 mixture has been also identified by other reported HC-SG catalysts, see Table SI2. Literature suggested that reaction temperatures higher than 250 °C and pressures of 30 bar·g should be used to achieve relatively high conversions (<42 %). A comparison of HC-SNG productivity of the estate-of-the-art of catalysts is shown in Fig. 11. For both cases, CO_2 or CO as a carbon source, the relationship between GHSV and HC-SG selectivity positioned the Co-Ni as a rentable material since significant productivity can be achieved by the implementation of technically feasible reaction conditions, leading to an HC-SG process economically profitable to be scaled-up at industrial levels. The productivity of the Co-Ni was around $8.08x10^2$ mL/g_{cat}·h using CO_2 and $5.15x10^3$ mL/g_{cat}·h using CO.

4. Conclusions

In this work, HC-SG synthesis was performed over a series of bimetallic Co-X (X = Ni, Pt and Fe) catalysts for the selective production of CH_4 and $C_2 - C_4$ hydrocarbons from CO_2 and CO as carbon sources. Catalytic results indicated that the utilization of CO as carbon source is very positive in both conversion and C_2-C_4 hydrocarbon selectivities. Among catalysts, Co-Ni was the most promising catalyst for production of HC-SG. Therefore, the strategy of adding a second metal proved to the positive. At H_2/CO = 3, T = 250 °C, and P = 10 bar·g, very interesting selectivities to CH_4 (40.01 %) and C_2–C_4 hydrocarbons (50.04 %) were obtained, with a reduced selectivity to CO_2 (5.05 %) and C_{5+} (4.89 %) formation. In this direction, a competitive HC-SG with a heating value of

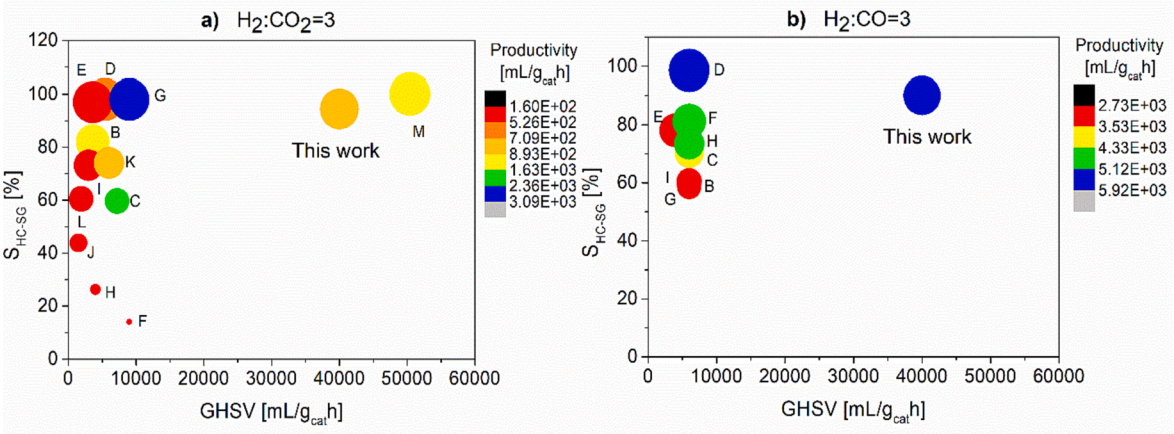

Fig. 11. Productivity comparison of the reported HC-SG catalysts using H_2:CO_x = 3 (x:1 and 2) showing the relationship between GHSV [mL/g_{cat}·h] and HC-SG Selectivity [%]. Productivity [mL/g_{cat}·h] = Y_{HC-SN} [%]*GHSV [mL/g_{cat}·h]. a) CO_2 as carbon source: A:Co-Ni [This work]; B:Fe-Co/K/Al_2O_3 [46]; C:10K13Fe_2-Co100Zr_2 [47]; D:$ZnGa_2O_4$/SAPO-34 [48]; E:ZnZrO/SAPO-34 [49]; F:In_2O_3/HZSM-5 [45]; G:In-Zr/SAPO-34 [50]; H:$NaFe_3O_4$/HZSM [51]; I:Fe-Zn-Zr@HZSM-5-Hbeta [52]; J:Cu-Zn-Al/modified-HB [53]; K:20Fe_2O_3-Al_2O_3 [10]; L:Fe-K/Al_2O_3 [12]; M: CeO_2–Pt@mSiO_2–Co [19]. b) CO as carbon source: A:Co-Ni [This work]; B:Fe_2O_3-R[9]; C:10Co/SiO_2[8]; D:10Co-6Mn-2.5Ru/Al_2O_3 [14]; E:50CFAL [15]; F: Fe–Co/Al_2O_3 [16]; G:FC15-400R [17]; H:5Co-15Fe-5Ni/γ-Al_2O_3 [21]; I:Fe-Zn [4].

57.90 MJ/Nm^3 was achieved using Co-Ni bimetallic catalysts.

The successful catalytic performance was attributed to the acid-basic sites formed on the catalyst surface by the synergic effects caused by the presence of La_2O_3 and CoNi alloy phases, which favours in the production of CH_4 and C_2-C_4 hydrocarbons under lower temperatures. Besides, the bimetallic Ni-Co catalyst showed higher reducibility (73.82 %) and active metal content (9.65x10^{-6}mmol/g). The findings from this study contribute to our understanding of the low temperature CO_2 and CO hydrogenation activities of La_2O_3 promoted Co-X/Al_2O_3 based catalysts and provide insights for the design of materials for HC-SG production.

Bimetallic Co-Ni catalyst can be used as a benchmark to optimize or design novel reactor approaches for the HC-SG process intensification. In the case of using CO_2 as carbon source, an adapted HC-SG reactor concept, configured by two Co-X catalytic zones is proposed to promote the use of CO_2 as carbon source. A first Co-Pt catalytic zone operated at 200 °C to favour the conversion CO_2 to CO and CH_x (x = 1,2,3) species, followed by a second Co-Ni catalytic zone operated at 250 °C to achieve the conversion CO to HC-SG (CH_4 and C_2-C_4 hydrocarbons). However, further studies should be carried out for the validation of this reactor engineering concept in a full-scale reactor. In any case, the use of bimetallic catalysts is interesting to divert selectivity towards the most desired products on each occasion.

CRediT authorship contribution statement

Andreina Alarcón: Writing – original draft, Investigation, Formal analysis, Visualization. **Olatz Palma:** Investigation, Validation. **Elena Martín Morales:** Investigation, Formal analysis, Writing – review & editing. **Martí Biset-Peiró:** Methodology, Resources. **Teresa Andreu:** Conceptualization, Validation, Supervision, Funding acquisition, Writing – review & editing. **Jordi Guilera:** Writing – original draft, Conceptualization, Methodology, Resources, Supervision, Funding acquisition.

Declaration of Competing Interest

The authors declare that they have no known competing financial interests or personal relationships that could have appeared to influence the work reported in this paper.

Data availability

Data will be made available on request.

Acknowledgement

This work was supported by project TED2021-132365B-I00, funded by MCIN/AEI/10.13039/ 501100011033 and by the European Union "NextGenerationEU"/PRTR and PID2019-108136RB-C33 (MCIN/AEI/ 10.13039/501100011033). Andreina is grateful for support by the Margarita Sala Grant funded by the University of Barcelona (UNI/551/ 2021). The authors thank SASOL for kindly providing alumina support material (Puralox). Authors kindly thank Dr. Albert Llorente for assistance with the characterization of materials.

Appendix A. Supplementary data

Supplementary data to this article can be found online at https://doi.org/10.1016/j.fuel.2023.127726.

References

[1] Guilera J, Filipe M, Montesó A, Mallol I, Andreu T. Carbon footprint of synthetic natural gas through biogas catalytic methanation. J Clean Prod 2021;287:125020. https://doi.org/10.1016/j.jclepro.2020.125020.

[2] Wu P, Sun J, Abbas M, Wang P, Chen Y, Chen J. Hydrophobic SiO2 supported Fe-Ni bimetallic catalyst for the production of high-calorie synthetic natural gas. Appl Catal A 2020;590:117302. https://doi.org/10.1016/j.apcata.2019.117302.

[3] MarketWatch. Liquefied Petroleum Gas (LPG) Market Share, Size 2022 Comprehensive Insights, Future Demand, Emerging Trends, Industry Overview, Business Strategies, Supply Demand Scenario, and Regional Forecast to 2024. March 2 2022.

[4] Lee YH, Lee D-W, Kim H, Choi HS, Lee K-Y. Fe–Zn catalysts for the production of high-calorie synthetic natural gas. Fuel 2015;159:259–68. https://doi.org/10.1016/j.fuel.2015.06.076.

[5] The National Institute of Standards and Technology from U.S. Department of Commerce. NIST Chemistry WebBook 2022. https://webbook.nist.gov/chemistry/.

[6] Jo SB, Chae HJ, Kim TY, Lee CH, Oh JU, Kang S-H, et al. Selective CO hydrogenation over bimetallic Co-Fe catalysts for the production of light paraffin hydrocarbons (C2–C4): Effect of H2/CO ratio and reaction temperature. Catal Commun 2018;117:74–8.

[7] Schulz H. Comparing Fischer-Tropsch synthesis on iron- and cobalt catalysts. The dynamics of structure and function. vol. 163. Elsevier B.V.; 2007. doi: 10.1016/S0167-2991(07)80479-4.

[8] Kim TY, Jo SB, Lee CH, Kang S-H, Kim JW, Lee SC, et al. Effect of reducibility on the performance of Co-based catalysts for the production of high-calorie synthetic natural gas. Korean J Chem Eng 2020;37(10):1690–8.

[9] Lee YH, Lee KY. Effect of surface composition of Fe catalyst on the activity for the production of high-calorie synthetic natural gas (SNG). Korean J Chem Eng 2017;34:320–7. https://doi.org/10.1007/s11814-016-0272-6.

[10] De la Rosa-Priego FA, Gutierrez-López ED, Zepeda TA, Acosta-Alejandro M, Venezia AM, Fuentes-Moyado S, et al. Enhanced CO2 Hydrogenation to C2+ Hydrocarbons over Mesoporous x %Fe2O3 –Al2O3 Catalysts. Ind Eng Chem Res 2021;60(51):18660–71.

[11] Ishigaki Y, Uba M, Nishida S, Inui T. Application of CoMn2O3Ru catalyst to the process for producing high-calorie substitute natural gas from coke oven gas. Appl Catal 1989;47:197–208. https://doi.org/10.1016/S0166-9834(00)83228-5.

[12] Riedel T, Claeys M, Schulz H, Schaub G, Nam S-S, Jun K-W, et al. Comparative study of Fischer-Tropsch synthesis with H2/CO and H2/CO2 syngas using Fe- and Co-based catalysts. Appl Catal A 1999;186(1-2):201–13.

[13] Qi Z, Chen L, Zhang S, Su J, Somorjai GA. A mini review of cobalt-based nanocatalyst in Fischer-Tropsch synthesis. Appl Catal A 2020;602:117701. https://doi.org/10.1016/j.apcata.2020.117701.

[14] Lee YH, Kim H, Choi HS, Lee D-W, Lee K-Y. Co-Mn-Ru/Al2O3 catalyst for the production of high-calorific synthetic natural gas. Korean J Chem Eng 2015;32:2220–6. https://doi.org/10.1007/s11814-015-0052-8.

[15] Kim TY, Jo SB, Woo JH, Lee JH, Dhanusuraman R, Lee SC, et al. Investigation of Co–Fe–Al Catalysts for High-Calorific Synthetic Natural Gas Production: Pilot-Scale Synthesis of Catalysts. Catalysts 2021;11(1):105.

[16] Lee J-Y, Jun K-W, Kang SC, Zhang C, Kwak G, Park J-M, et al. Fe–Co/alumina catalysts for production of high calorific synthetic natural gas: Effect of Fe/Co ratio. J Ind Eng Chem 2018;66:396–403.

[17] Lee YH, Lee D-W, Lee K-Y. Production of high-calorie synthetic natural gas using copper-impregnated iron catalysts. J Mol Catal A Chem 2016;425:190–8. https://doi.org/10.1016/j.molcata.2016.10.013.

[18] Nie X, Wang H, Liang Z, Yu Z, Zhang J, Janik MJ, et al. Comparative computational study of CO2 dissociation and hydrogenation over Fe-M (M = Pd, Ni, Co) bimetallic catalysts: The effect of surface metal content. J CO2 Util 2019;29:179–95.

[19] Xie C, Chen C, Yu Yi, Su Ji, Li Y, Somorjai GA, et al. Tandem Catalysis for CO2 Hydrogenation to C2–C4 Hydrocarbons. Nano Lett 2017;17(6):3798–802.

[20] Sun J, Chen Z, Xue Y, Chen J. Design and construction of Ni 3–x CoxO4 nanorods grown on Ni foam for tuning synthetic natural gas heating values. New J Chem 2018;42:2743–9. https://doi.org/10.1039/C7NJ03904B.

[21] Kim T-Y, Jo S, Lee Y, Kang S-H, Kim J-W, Lee S-C, et al. Influence of Ni on Fe and Co-Fe Based Catalysts for High-Calorific Synthetic Natural Gas. Catalysts 2021;11(6):697.

[22] Guilera J, del Valle J, Alarcón A, Díaz JA, Andreu T. Metal-oxide promoted Ni/Al2O3 as CO2 methanation micro-size catalysts. J CO2 Util 2019;30:11–7. https://doi.org/10.1016/j.jcou.2019.01.003.

[23] Guilera J, Díaz-López JA, Berenguer A, Biset-Peiró M, Andreu T. Fischer-Tropsch synthesis: Towards a highly-selective catalyst by lanthanide promotion under relevant CO2 syngas mixtures. Appl Catal A 2022;629:118423. https://doi.org/10.1016/j.apcata.2021.118423.

[24] Guilera J, Andreu T, Alarcón A, Badia J. A micro-catalyst, A process for preparing thereof and use thereof. P33585EP00 2021.

[25] Thommes M, Kaneko K, Neimark A V., Olivier JP, Rodriguez-Reinoso F, Rouquerol J, et al. Physisorption of gases, with special reference to the evaluation of surface area and pore size distribution (IUPAC Technical Report). Pure and Applied Chemistry 2015;87:1051–69. doi: 10.1515/pac-2014-1117.

[26] Díaz-López JA, Guilera J, Biset-Peiró M, Enache D, Kelly G, Andreu T. Passivation of Co/Al2O3 Catalyst by Atomic Layer Deposition to Reduce Deactivation in the Fischer-Tropsch Synthesis. Catalysts 2021;11:732. https://doi.org/10.3390/catal11060732.

[27] Zhao L, Mu X, Liu T, Fang K. Bimetallic Ni-Co catalysts supported on Mn-Al oxide for selective catalytic CO hydrogenation to higher alcohols. Cat Sci Technol 2018;8:2066–76. https://doi.org/10.1039/c7cy02555f.

[28] Araújo JCS, Oton LF, Bessa B, Neto ABS, Oliveira AC, Lang R, et al. The role of Pt loading on La2O3-Al2O3 support for methane conversion reactions via partial oxidation and steam reforming. Fuel 2019;254:115681. doi: 10.1016/j.fuel.2019.115681.

[29] Al -Fatesh AS, Kasim SO, Ibrahim AA, Al-Awadi AS, Abasaeed AE, Fakeeha AH, et al. Catalytic methane decomposition over ZrO2 supported iron catalysts: Effect of WO3 and La2O3 addition on catalytic activity and stability. Renew Energy 2020; 155:969–78.
[30] Cai Z, Li J, Liew K, Hu J. Effect of La2O3-dopping on the Al2O3 supported cobalt catalyst for Fischer-Tropsch synthesis. J Mol Catal A Chem 2010;330:10–7. https://doi.org/10.1016/j.molcata.2010.06.025.
[31] Kaneko S, Izuka M, Takahashi A, Ohshima M, Kurokawa H, Miura H. Pt dispersion control in Pt/SiO 2 by calcination temperature using chloroplatinic acid as catalyst precursor. Appl Catal A 2012;427–428:85–91. https://doi.org/10.1016/j.apcata.2012.03.033.
[32] Choi YH, Jang YJ, Park H, Kim WY, Lee YH, Choi SH, et al. Carbon dioxide Fischer-Tropsch synthesis: A new path to carbon-neutral fuels. Applied Catalysis B: Environmental 2017;202:605–10. doi: 10.1016/j.apcatb.2016.09.072.
[33] Das T, Deo G. Synthesis, characterization and in situ DRIFTS during the CO2 hydrogenation reaction over supported cobalt catalysts. J Mol Catal A Chem 2011; 350:75–82. https://doi.org/10.1016/j.molcata.2011.09.008.
[34] Bobadilla LF, Egaña A, Castillo R, Romero-Sarria F, Centeno MA, Sanz O, et al. Understanding the promotional effect of Pt/CeO2 in cobalt-catalyzed Fischer-Tropsch synthesis using operando infrared spectroscopy at moderated pressures. Fuel 2022;312:122964. doi: 10.1016/j.fuel.2021.122964.
[35] Santos J, Bobadilla L, Centeno M, Odriozola J. Operando DRIFTS-MS Study of WGS and rWGS Reaction on Biochar-Based Pt Catalysts: The Promotional Effect of Na. C 2018;4:47. https://doi.org/10.3390/c4030047.
[36] Cárdenas-Arenas A, Quindimil A, Davó-Quiñonero A, Bailón-García E, Lozano-Castelló D, De-La-Torre U, et al. Isotopic and in situ DRIFTS study of the CO2 methanation mechanism using Ni/CeO2 and Ni/Al2O3 catalysts. Appl Catal B 2020;265:118538.
[37] Gholami Z, Tišler Z, Rubáš V. Recent advances in Fischer-Tropsch synthesis using cobalt-based catalysts: a review on supports, promoters, and reactors. Catal Rev 2021;63:512–95. https://doi.org/10.1080/01614940.2020.1762367.
[38] Manoilova OV, Podkolzin SG, Tope B, Lercher J, Stangland EE, Goupil J-M, et al. Surface Acidity and Basicity of La2O3, LaOCl, and LaCl3 Characterized by IR Spectroscopy, TPD, and DFT Calculations. J Phys Chem B 2004;108(40):15770–81.
[39] Yamamoto T, Hatsui T, Matsuyama T, Tanaka T, Funabiki T. Structures and Acid−Base Properties of La/Al2O3 Role of La Addition to Enhance Thermal Stability of γ-Al2O3. Chem Mater 2003;15:4830–40. https://doi.org/10.1021/cm034732c.
[40] Lemaitre L, Berliet A, Maury S, Rivallan M. Surface modifications of cobalt Fischer Tropsch catalyst followed by operando DRIFT and chemometrics. Catal Today 2017;283:172–5. https://doi.org/10.1016/j.cattod.2016.02.033.
[41] Schweicher J, Bundhoo A, Frennet A, Kruse N, Daly H, Meunier FC. DRIFTS/MS studies during chemical transients and SSITKA of the CO/H2 reaction over Co-MgO catalysts. J Phys Chem C 2010;114:2248–55. https://doi.org/10.1021/jp909754w.
[42] Sonal, Pant KK, Upadhyayula S. An insight into the promotional effect on Fe-Co bimetallic catalyst in the Fischer Tropsch reaction: A DRIFTS study. Fuel 2020;276: 118044. doi: 10.1016/j.fuel.2020.118044.
[43] Concepción P, Corma A, Silvestre-Albero J, Franco V, Chane-Ching JY. Chemoselective Hydrogenation Catalysts: Pt on Mesostructured CeO2 Nanoparticles Embedded within Ultrathin Layers of SiO2 Binder. J Am Chem Soc 2004;126:5523–32. https://doi.org/10.1021/ja031768x.
[44] Wang S, Yin Q, Guo J, Zhu L. Influence of Ni Promotion on Liquid Hydrocarbon Fuel Production over Co/CNT Catalysts. Energy Fuel 2013;27:3961–8. https://doi.org/10.1021/ef400726m.
[45] Gao P, Li S, Bu X, Dang S, Liu Z, Wang H, et al. Direct conversion of CO2 into liquid fuels with high selectivity over a bifunctional catalyst. Nat Chem 2017;9(10): 1019–24.
[46] Satthawong R, Koizumi N, Song C, Prasassarakich P. Light olefin synthesis from CO2 hydrogenation over K-promoted Fe-Co bimetallic catalysts. Catal Today 2015; 251:34–40. https://doi.org/10.1016/j.cattod.2015.01.011.
[47] Li W, Zhang A, Jiang X, Janik MJ, Qiu J, Liu Z, et al. The anti-sintering catalysts: Fe–Co–Zr polymetallic fibers for CO2 hydrogenation to C2 = –C4 = –rich hydrocarbons. J CO2 Util 2018;23:219–25.
[48] Liu X, Wang M, Zhou C, Zhou W, Cheng K, Kang J, et al. Selective transformation of carbon dioxide into lower olefins with a bifunctional catalyst composed of ZnGa2O4 and SAPO-34. Chem Commun 2018;54(2):140–3.
[49] Li Z, Wang J, Qu Y, Liu H, Tang C, Miao S, et al. Highly Selective Conversion of Carbon Dioxide to Lower Olefins. ACS Catal 2017;7(12):8544–8.
[50] Gao P, Dang S, Li S, Bu X, Liu Z, Qiu M, et al. Direct Production of Lower Olefins from CO2 Conversion via Bifunctional Catalysis. ACS Catal 2018;8(1):571–8.
[51] Wei J, Ge Q, Yao R, Wen Z, Fang C, Guo L, et al. Directly converting CO 2 into a gasoline fuel. Nat Commun 2017;8(1). https://doi.org/10.1038/ncomms15174.
[52] Wang X, Yang G, Zhang J, Chen S, Wu Y, Zhang Q, et al. Synthesis of isoalkanes over a core (Fe-Zn-Zr)-shell (zeolite) catalyst by CO2 hydrogenation. Chem Commun 2016;52(46):7352–5.
[53] Behrens M, Studt F, Kasatkin I, Kühl S, Hävecker M, Abild-pedersen F, et al. Industrial Catalysts 2012;759:893–7.